Mechanism of Gating of T-Type Calcium Channels

CHINFEI CHEN and PETER HESS

From the Department of Cellular and Molecular Physiology and Program in Neuroscience, Harvard Medical School, Boston, Massachusetts 02115

ABSTRACT We have analyzed the gating kinetics of T-type Ca channels in 3T3 fibroblasts. Our results show that channel closing, inactivation, and recovery from inactivation each include a voltage-independent step which becomes rate limiting at extreme potentials. The data require a cyclic model with a minimum of two closed, one open, and two inactivated states. Such a model can produce good fits to our data even if the transitions between closed states are the only voltage-dependent steps in the activating pathway leading from closed to inactivated states. Our analysis suggests that the channel inactivation step, as well as the direct opening and closing transitions, are not intrinsically voltage sensitive. Single-channel recordings are consistent with this scheme. As expected, each channel produces a single burst per opening and then inactivates. Comparison of the kinetics of T-type Ca current in fibroblasts and neuronal cells reveals significant differences which suggest that different subtypes of T-type Ca channels are expressed differentially in a tissue specific manner.

INTRODUCTION

T-type Ca channels, also called "low voltage activated" (Carbone and Lux, 1984; Bossu et al., 1985; Kostyuk et al., 1988), "I_{fast}" (Bean, 1985), or "slowly deactivating" (Armstrong and Matteson, 1985), are a class of voltage-activated Ca channels found in a wide variety of excitable and nonexcitable cells (Tsien et al., 1988; Bean, 1989*a*; Hess, 1990). T-type currents are characterized by a transient time course during voltage clamp depolarizations, and a relatively negative voltage range of activation and steady-state inactivation. The postulated physiological roles of T-type calcium channels include a contribution to the pacemaker potential in cardiac cells (Hagiwara et al., 1988), maintenance of repetitive firing in central neurons (Llinas and Yarom, 1981; Coulter et al., 1989), and control of hormonal secretion in some endocrine cells (DeRiemer and Sakmann, 1986; Cohen et al., 1988). Correlations between T-type channel expression and oncogenic transformation (Chen et al., 1988), cell adherence (Garber et al., 1990), development (Yaari et al., 1987; Sturek and Hermsmeyer, 1986; Beam and Knudson, 1988), and differentiation (Caffrey et al., 1987) suggest additional physiological roles of this Ca channel type that remain poorly understood.

Address reprint requests to Dr. Peter Hess, Department of Cellular and Molecular Physiology, Harvard Medical School, 25 Shattuck Street, Boston, MA 02115

J. GEN. PHYSIOL. © The Rockefeller University Press · 0022-1295/90/09/0603/28 $2.00
Volume 96 September 1990 603–630

In this paper, we use a combination of whole-cell and single-channel recordings to present an analysis of the gating kinetics of T-type Ca channels in fibroblasts. We find that although channel deactivation, inactivation and reactivation kinetics in whole-cell currents are voltage dependent, the rate-limiting steps for each of these transitions become voltage independent at extreme potentials. Our data are consistent with recent single-channel recordings from cardiac T-type Ca channels (Droogmans and Nilius, 1989). We interpret our findings with a kinetic scheme in which activation and inactivation are coupled, but where only activation is voltage dependent, analogous to models proposed initially for the kinetics of Na channel gating (Bezanilla and Armstrong, 1977; Bean, 1981; Aldrich et al., 1983; Gonoi and Hille, 1987; Kirsch and Brown, 1989; Cota and Armstrong, 1989). Furthermore, we conclude that the direct opening and closing transitions are also voltage independent. Our data require a minimum of two closed, one open, and two inactivated states. The resulting cyclic model provides a good fit to the time course and steady-state inactivation of the currents, and allows us to extract the voltage dependence of the potential-sensitive transitions. Surprisingly, we find that T-type currents from neuronal cells differ significantly from those recorded in fibroblasts. The neuronal currents activate and inactivate more slowly and show a more shallow voltage dependence. Moreover, even with adjusted parameters, the model which fits fibroblast T-type currents cannot adequately reproduce neuronal T-type currents. Thus, T-type channels either represent a heterogeneous group of Ca channels made up of different subtypes, or their function depends critically on the cellular environment.

METHODS

Tissue Culture

Swiss and NIH 3T3 fibroblasts kindly provided by Drs. G. Cooper, H. Green, and T. Roberts were grown in plastic petri dishes in Dulbecco's modified Eagle's medium (DMEM) with 10% calf serum at 37°C, and fed every 2 d. The NG108 neuroblastoma-glioma cell line was grown in DMEM with 10% fetal calf serum. Superior cervical ganglion cells were obtained as previously described (Plummer et al., 1989).

For whole-cell experiments which required electrically uncoupled single cells, cells grown in culture dishes were exposed to medium containing 0.1% trypsin and 0.5 mM EDTA for 2–5 min at room temperature. The cells were then triturated and resuspended in DMEM-containing serum. Drops of the suspended cells were placed into the experimental chamber for electrical recordings. For single-channel experiments cells were grown on glass coverslips that were cut into small pieces for transfer into the experimental chamber.

Patch Clamp Recordings

Whole-cell calcium currents and unitary calcium channel recordings were obtained as described by Hamill et al. (1981). Patch pipettes were pulled from Boralex hematocrit micropipettes (P5251, USA Scientific Plastics, Ocala, FL), coated with Sylgard (Dow Corning Corp., Midland, MI), and firepolished. Current signals were recorded with a custom-built patch clamp amplifier (V. Pantani and associates, Yale University) or a model 3900 (DAGAN Corp., Minneapolis, MN). Currents were filtered with an eight-pole Bessel filter at a

half-power frequency of 1 kHz (unless otherwise noted) and sampled at a rate five times the filter frequency. The signals were stored and analyzed on a PDP 11-73 laboratory computer.

Solutions for whole-cell recordings had the following composition: external solution—20 mM Ba acetate 135 mM tetraethylammonium (TEA)-aspartate, 10 mM HEPES, pH 7.5; and internal solution—135 mM Cs-aspartate, 10 mM EGTA, 10 mM HEPES, 5 mM $MgCl_2$, 4 mM ATP, pH 7.5. These solutions were designed to eliminate outward K currents (Ba, TEA, and Cs) and Cl^- currents (acetate and aspartate). For unitary channel recordings, the membrane potential outside the bath was zeroed (Hess et al., 1986) with the following bathing solution: 140 mM K-aspartate, 10 mM EGTA, 10 mM HEPES, titrated to pH 7.4 with KOH. The pipette solution contained 110 mM $CaCl_2$ or 110 mM $BaCl_2$ and 10 mM HEPES, pH 7.5. All recordings were done at room temperature (22°C). Liquid junction potentials ranged between 5 and 10 mV and were not corrected.

Data Analysis

All current records are shown after digital subtraction of linear leak and capacitance currents. Capacitance and series resistance were determined from the time course of a capacitative transient sampled at 100 kHz without filtering. The series resistance remaining after maximal compensation ranged between 1 and 5 MΩ. The timecourse of whole-cell T-currents and tail currents was fit to exponential curves by χ^2 minimization. Voltage errors were calculated from the series resistance and the amplitude of the total current before leak subtraction. The maximal tolerated voltage error was 2 mV.

Single-channel recordings were idealized for the construction of histograms by a midline crossing detector, and histograms were fitted to single or double exponential curves by χ^2 minimization.

Model Calculations

The time course of the open time probability, $p_o(t)$, for the model shown as Scheme 3a in the text was computed by numerical integration of the simultaneous differential equations with the use of a fourth-order Runge-Kutta routine. The starting conditions were that at time 0 at negative holding potentials the channel was at equilibrium between states C_1 and I_1, such that the probability of finding a channel in C_1 at time 0 is $k_r/(k_r + k_{-r})$. For steady-state inactivation curves, the steady-state probabilities of each state at the holding potential were calculated and used as starting values for the computation of the time course of the open probability. Steady-state values of the probabilities were calculated by the method of King and Altman (1956).

RESULTS

T-Type Currents in Fibroblasts

We have previously shown that 3T3 fibroblasts contain T-type and L-type Ca channels which carry the only voltage- and time-dependent inward currents in these cells (Chen et al., 1988). In some fibroblasts, particularly after prolonged whole-cell recordings, T-type currents largely dominate the whole-cell current, because of the well-known rundown of L-type, but not T-type Ca currents (Nilius et al., 1985; Carbone and Lux, 1987*a*). This allowed us to study the kinetics of T-type currents even at potentials (> -10 mV) where overlap with L-type currents was unavoidable.

Fig. 1 shows a family of currents recorded from a holding potential of -80 mV during test depolarizations to potentials between -60 and $+120$ mV. Inward

currents become detectable at −50 mV and reach a peak at −20 mV. At potentials positive to +50 mV the current reverses sign. The inward currents carried by Ba, the positive value of the reversal potential, the activation at negative membrane potentials, and the rapid and virtually complete inactivation even with Ba as charge carrier are all expected properties for T-type Ca channels. For our kinetic treatment, we will assume that inactivation during a depolarization is essentially complete. This is justified since, over the voltage range where T-type current is recorded in isolation (−50 to −10 mV in Fig. 1), the leak subtracted currents decay to a value not measurably different from zero. The small, steady current shown in Fig. 1 at more positive potentials is carried by L-type channels, and can be subtracted by protocols in which L-type current is measured in isolation during voltage clamp steps from depolarized holding potentials (see, e.g., Bean, 1985; Chen et al., 1988).

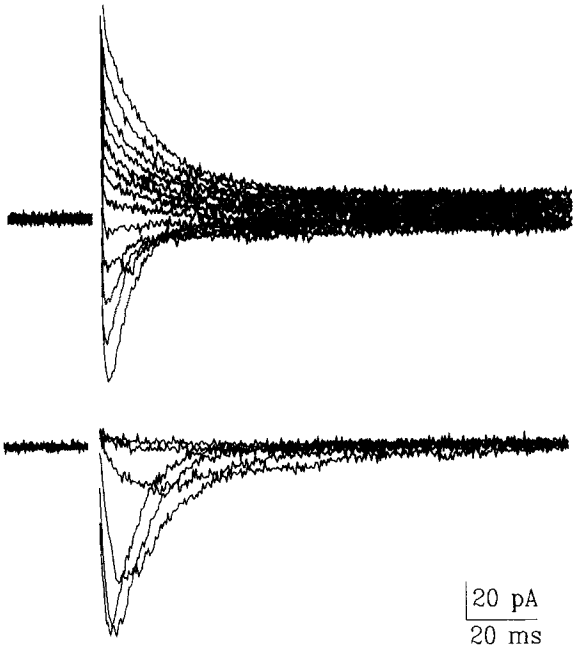

FIGURE 1. Whole-cell currents in 3T3 fibroblast carried through T-type Ca channels with 20 Ba as charge carrier. Holding potential −80 mV. Lower panel: Superimposed currents elicited by depolarizations ranging from −60 mV (smallest current) to −10 mV (largest inward current) in 10-mV increments. Upper panel: Currents elicited by depolarization ranging from 0 mV (lowest trace) to 120 mV (uppermost trace) in 10-mV increments. Cell T61B. In addition to the T-type current, this cell also contained a small L-type current (maximum of 9 pA at +20 mV) as assessed from a holding potential of −40 mV, which completely inactivated the T-type current (Chen et al., 1988).

Voltage Dependence of the Rate of Inactivation

The transient waveform of the current during a voltage clamp depolarization must result from transitions from closed to open and inactivated states. The minimal scheme is

$$C \underset{k_d}{\overset{k_a}{\rightleftharpoons}} O \xrightarrow{k_i} I$$

(Scheme 1)

where k_a is the rate constant for channel activation (opening), and k_d and k_i are the rate constants for deactivation (closing) and inactivation, respectively. k_a and k_d in Scheme 1 must be voltage dependent, otherwise the channel could not be closed at negative potentials. The remaining question concerns the voltage dependence of k_i. For Na channels, a number of reports (e.g., Bezanilla and Armstrong, 1977; Bean, 1981; Aldrich et al., 1983; Gonoi and Hille, 1987; Kirsch and Brown, 1989; Cota and Armstrong, 1989) have shown that the voltage dependence of inactivation of whole-cell currents can be derived from the voltage dependence of activation, rather

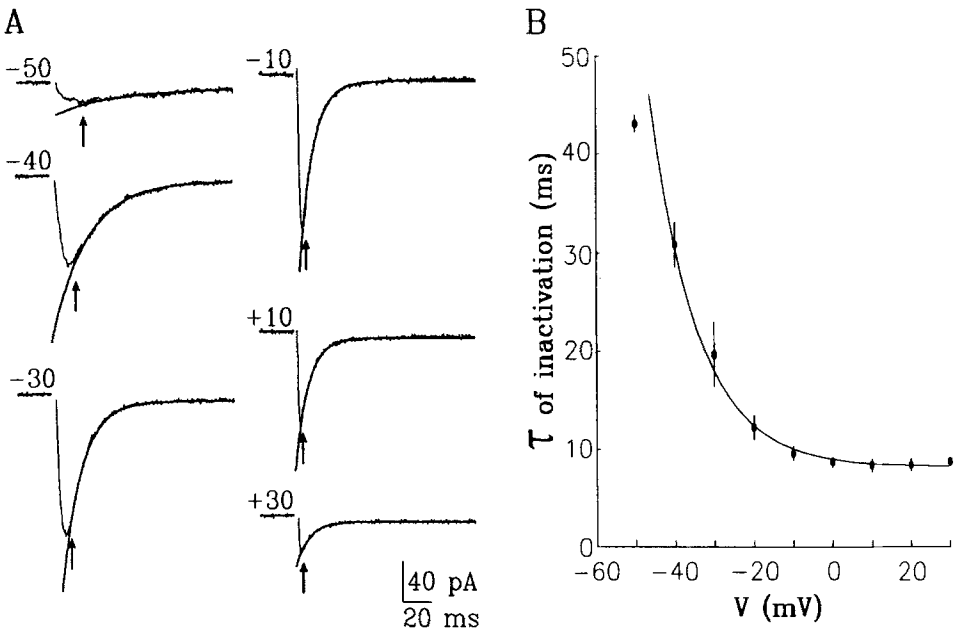

FIGURE 2. Voltage dependence of macroscopic inactivation. (*A*) Examples of fits (*solid line*) of the decay of T-type current to a single exponential. Holding potential −80 mV. Test potentials indicated above each trace. 20 mM Ba is the charge carrier. Arrows indicate the left-hand limit for the χ^2 exponential fit. Cell N80C. (*B*) Plot of time constant of inactivation vs. voltage. Data points are mean ± SEM from nine experiments. Smooth line indicates appoximately exponential voltage dependence of the time constants, with *e*-fold change per 12 mV and voltage independent offset of 9 ms.

than from a voltage-dependent value of k_i, as previously believed (Hodgkin and Huxley, 1952).

As shown in Fig. 2 *A*, the decay of the whole-cell T-type current can be well fitted by a single exponential over the entire voltage range. We tested for an inherent voltage dependence of k_i by plotting the measured time constant of inactivation (τ_i) as a function of the test potential. Following conventional rate theory, we will assume exponential voltage dependence for any single voltage-dependent rate constant. Thus, if k_i itself were voltage dependent, then τ_i should continue to decay with

increasing voltage, eventually reaching a value of 0 at infinitely positive potentials. Contrary to this prediction, τ_i reaches a voltage-independent value of about 10 ms at $V = 0$ mV (Fig. 2 *B*). We can interpret this result by noting that in a series of voltage-dependent and voltage-independent transitions the voltage-independent rate constants must become rate limiting at extreme voltages and thus apparent as the maximum rates at which the overall reaction can proceed. Thus, the finding that τ_i is

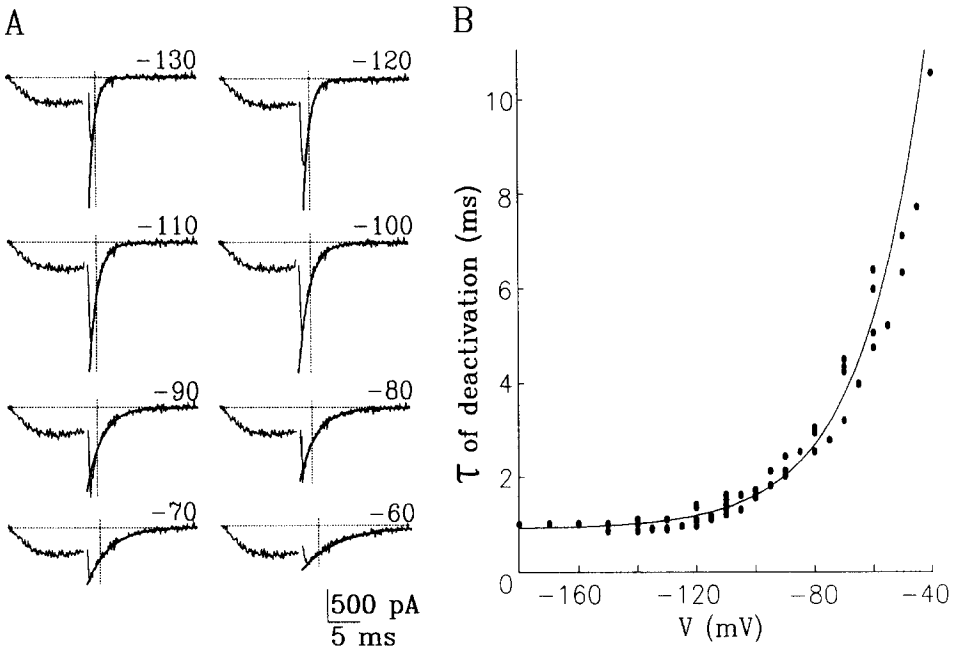

FIGURE 3. Voltage dependence of channel deactivation. (*A*) Examples of exponential fits (*solid line*) of tail currents elicited by repolarization to tail potentials indicated above each trace. Current was activated by a 14-ms depolarization to 35 mV. Currents sampled at 20 kHz and filtered at 5 kHz, recorded with integrating headstage (DAGAN 3900). Left-hand limit of χ^2 fit for each current trace indicated by vertical dashed line. Uncompensated series resistance 2.3 MΩ. The first 250 μs after repolarization are blanked because saturation of the A/D converter made correct subtraction of linear capacitative currents impossible during this time. 20 mM Ba is the charge carrier. Cell N95B, capacitance 105 pF. (*B*) Plot of time constant of deactivation vs. voltage of repolarization. Values obtained from two different cells. Smooth line indicates approximately exponential voltage dependence of the time constants, with *e*-fold change per 22 mV and voltage independent offset of 0.9 ms.

only voltage dependent over the potential range in which activation is slow enough to lead to a measurable delay in the peak current (compare Figs. 1 and 2 *B*), provides strong evidence that k_i itself is not voltage dependent and has a value of 150–200/s. The voltage dependence of macroscopic inactivation is thus caused by the slow and voltage-dependent delivery rate (activation) of channels to the open state.

The data illustrated in Fig. 2 agree qualitatively with previous reports of the voltage dependence of inactivation of the T-type channel in neurons (Fedulova et al.,

1985; Carbone and Lux, 1987*a*; Fox et al., 1987*a*; Akaike et al., 1989; Coulter et al., 1989), myeloma cells (Fukushima and Hagiwara, 1985), and cardiac cells (Bean, 1985; but see Hagiwara et al., 1988). In all these reports, a voltage-independent value of τ_i was found at positive test potentials, but its significance was not pointed out. We have noted that in a number of experiments on fibroblasts the time constant of inactivation decreases with increasing voltage but appears to increase again at voltages positive to the reversal potential (see, e.g., Fig. 1). In addition, after subtraction of linear components, the outward currents contain a more pronounced steady component than the inward currents. We have not attempted to test whether these kinetic effects seen during strong depolarizations reflect true properties of T-type channels or are caused by overlapping activation of residual, not completely blocked outward currents through other channels. We therefore limit our kinetic analysis to membrane potentials negative to the reversal potential.

Voltage Dependence of Channel Closing: Deactivation

We applied the same principle of using extreme potentials to unmask a voltage-independent rate constant to look for voltage-independent transitions during channel closing, measured as the rate of tail current deactivation after an activating prepulse. Single exponentials provided satisfactory fits to the tail currents over a large voltage range (-40 to -200 mV, see Fig. 3 *A*). A plot of the time constants of tail current decay (τ_d) as a function of voltage revealed that deactivation reaches a voltage independent rate of ~1,000/s ($\tau_d = 1$ ms) at -120 mV (Fig. 3 *B*). In this series of experiments, it was important to rule out the possibility that the apparent saturation of τ_d was not simply due to a progressive voltage error introduced by the large capacitative currents flowing across the series resistance of the patch pipette. We assessed the magnitude of the errors by frequent monitoring of the series resistance remaining after maximal compensation. The beginning of the exponential fit was restricted to the time point at which the total membrane current had decayed to an amplitude which gave a voltage error of <2 mV. The apparent saturation of the time constant of deactivation is also unlikely to result from an artifactually slow voltage clamp. In the three cells analyzed, the capacitative current transients decayed with time constants of 110, 130, and 240 μs respectively, much faster than the maximal rate of tail current decay.

The results of Fig. 3 strongly suggest the presence of a voltage-independent closing rate constant with a value of ~1,000/s. Thus we must expand Scheme 1 to include at least one more closed state:

$$C \underset{k_d(V)}{\overset{k_a(V)}{\rightleftharpoons}} C \underset{k_c}{\overset{k_o}{\rightleftharpoons}} O \xrightarrow{k_i} I$$

(Scheme 2)

Here, k_o and k_c are the opening and closing rate constants, respectively. We have no direct evidence concerning the voltage dependence of k_o, but will assume that like k_c, k_o is also voltage independent. Scheme 2 predicts that single-channel openings should occur in bursts, consistent with previous single-channel measurements

(Carbone and Lux, 1984, 1987*b*; Nilius et al., 1985) and our own data shown below. Dependent on the relative values of the rate constants in Scheme 2, tail currents might be expected to be composed of more than one decaying exponential component. This, however, does not invalidate the conclusions drawn from Fig. 3, since the main point here is to show that at negative values tail deactivation becomes voltage independent.

When differences in temperature and solution are taken into consideration, our results of tail current deactivation in fibroblasts are remarkably similar to those from other studies of T-current deactivation in sensory neurons (Carbone and Lux, 1987*a*) and clonal pituitary cells (Matteson and Armstrong, 1986; see Discussion and Table II). As expected from the plot shown in Fig. 3, previous studies, limited to potentials positive to −100 mV (Matteson and Armstrong, 1986; Carbone and Lux, 1987*a*), did not find saturation of tail current deactivation.

Voltage Dependence of Recovery

A reasonable model for gating of a channel that inactivates during a test depolarization and returns from inactivation without reopening must be cyclic (see also Discussion).

In order to learn more about the return of inactivated channels to the closed states, we studied the recovery from inactivation. Fig. 4*a* shows examples of T-type currents elicited after varying intervals at negative potentials after a prepulse from −80 to −20 mV which had fully inactivated the current. The fraction of current recovered, calculated as the ratio of the peak currents elicited by the second pulse and the prepulse, is plotted with respect to the length of the reactivating interpulse interval in Fig. 4 *B*. The time dependence of recovery can be fitted by an exponential time course with a time constant (τ_r) of 90 ms. The voltage dependence of τ_r is shown in Fig. 4 *C*. τ_r decreases with hyperpolarization of the interpulse potential, but reaches a voltage independent value of ~100 ms at interpulse voltages negative to −80 mV. Therefore, we conclude that, like deactivation and inactivation, the pathway from the inactivated state to the closed state must involve at least one voltage-independent transition which becomes rate limiting at very negative potentials. The channel must undergo at least two consecutive transitions between the inactivated and the resting states. One of these transitions is voltage dependent, the other one is not. We therefore expand our kinetic scheme in the following way:

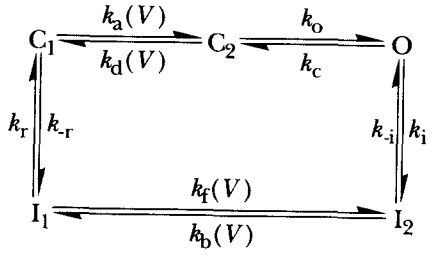

(Scheme 3a)

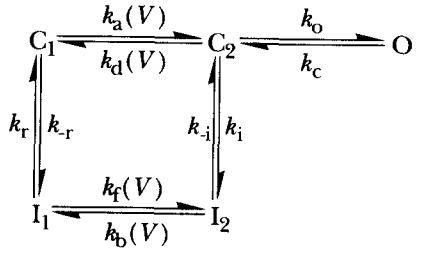

(Scheme 3b)

As long as k_o, k_c, k_i and k_{-i} are all voltage independent, neither whole-cell currents nor single-channel recordings can help distinguish between Schemes 3a and 3b. We therefore consider the two schemes formally equivalent and have used Scheme 3a for our numerical calculations. Several alternatives to Scheme 3 exist. We mention them in the Discussion and explain there why we consider them less likely to account for our data.

Recovery of the T-type current in mouse 3T3 fibroblasts is similar to that reported in cardiac cells (Hagiwara et al., 1988) and about 2–10 times faster than that

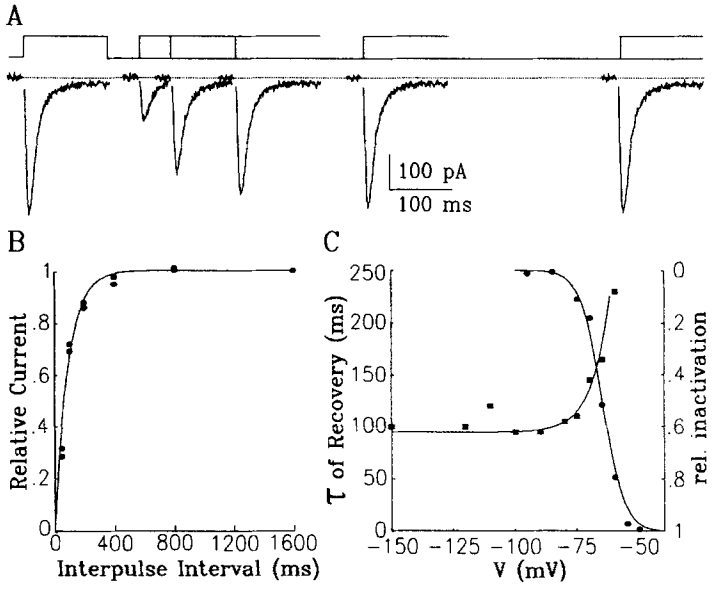

FIGURE 4. Voltage dependence of recovery from inactivation. (*A*) T-type Ba currents, following the end of an initial depolarizing pulse (l. trace) at intervals of 50, 100, 200, 400, and 800 ms. Interpulse potential −80 mV, test potential −20 mV. 20 mM Ba is the charge carrier. Cell N97B (*B*) Plot of the relative peak current from *A* as a function of interpulse interval. Relationship is fit by a single exponential with a time constant of 90 ms (*solid line*). (*C*) Plot of time constant of recovery vs. interpulse voltage (rectangles, right axis). Data are mean values from two cells. Smooth line indicates exponential voltage dependence with *e*-fold change per 7 mV and voltage independent offset of 95 ms. Circles and right axis: Steady-state inactivation curve from cell N97B. Smooth line is drawn according to equation: relative inactivation = $1/[1 + \exp(V_{1/2} - V)/k]$ with $V_{1/2} = -65$ mV and $k = 4.3$ mV.

reported in neurons (Carbone and Lux, 1987*a*; Akaike et al., 1989; Coulter et al., 1989; see also Discussion and Table II). Our data are consistent with the findings of Coulter et al (1989) who report that recovery of the T-current in central neurons is insensitive to interpulse voltages between −92 and −112 mV.

A Quantitative Description of T-Type Channel Gating

We have explored whether Scheme 3, which we consider the simplest model qualitatively compatible with our results, can also fit our data quantitatively.

Although this model has 10 adjustable parameters (nine rate constants, one factor to describe the voltage dependence), the values of most parameters are in fact severely constrained if all the data are to be reproduced satisfactorily. For reasons of microscopic balance, all rate constants in Scheme 3 must have finite values, and the voltage dependence of the equilibria between the two closed and the inactivated states must be the same. Our choice of parameters are guided by the following considerations. k_i has to have a value close to the saturating value of the rate of inactivation, determined in Fig. 2. k_{-i} must be much smaller than k_i to assure almost complete inactivation during a pulse. k_c has a value similar to the fastest rate of deactivation measured at negative potentials (Fig. 3). k_0 must be large (>1,000/s), to be compatible with the short closed times within bursts of openings (see below). k_r and k_{-r} determine the equilibrium between channels in the available (C_1) and unavailable (I_1) state at negative potentials. Since single-channel recordings revealed traces with detectable openings in roughly one out of four depolarizations (see below), we set k_r equal to $k_{-r}/3$. The sum of $k_r + k_{-r}$ determines the rate of macroscopic relaxation of the equilibrium between states C_1 and I_1 at negative potentials. Thus the sum of $k_r + k_{-r}$ was set to a value which fits the observed limiting rate of recovery at negative potentials. The values of k_a and k_b, and their voltage dependence, were adjusted in order to obtain the best fit to the time course of the current for test potentials ranging from -50 to $+10$ mV. The necessity for microscopic reversibility dictated the ratio between k_f and k_b. Consistent with conventional rate theory, we assumed exponential dependence of rate constants on voltage:

$$k = k(V = 0) \cdot \exp(zqVF/RT), \tag{1}$$

where $k(V = 0)$ is the voltage-independent value of k at 0 mV, $z = 1$ for k_a and k_f and $z = -1$ for k_d and k_b. F, R, and T have their usual values and q is the equivalent charge moved across the membrane electric field in the transition. The same charge was assumed to be moved for the forward and backward transition in each pair of voltage-dependent rate constants.

Fig. 5 *A* shows that with the values of the rate constants given in Table I, the model provides a good fit to the time course of the whole-cell currents. Since this model specifies the kinetic behavior of T-type current over the entire voltage range, it should also reproduce the measured steady-state inactivation curve and produce a reasonable activation curve of the peak current. This is indeed the case, as illustrated in Fig. 5 *B*. Both the midpoint and the steepness of the steady-state inactivation curve are well predicted. The calculated values of the open probability at the time of the peak current (p_{peak}) are shown normalized to the saturating value at positive potentials. When the measured peak currents of the current–voltage relation are divided by the values of p_{peak}, a curve corresponding to the open-channel current–voltage relation is expected. The predicted curve is shown in Fig. 5 *C*. It is compatible with known current–voltage relations of open Ca channels (Hess et al., 1986), which have a linear slope at negative potentials and show gradual inward rectification as the reversal potential is approached.

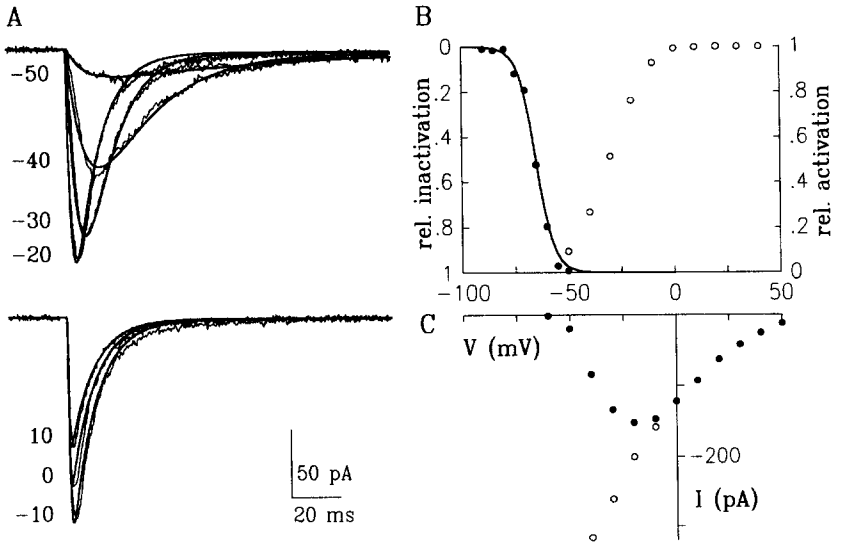

FIGURE 5. Model fit of T-type Ba currents in 3T3 fibroblasts. (*A*) Current records (noisy traces) and superimposed model fits for depolarizations from a holding potential of −80 mV to the test potentials indicated next to each current trace. Data from cell N80C. Model fit obtained with Scheme 3a (see text) and parameters listed in Table I. (*B*) Fit of steady-state inactivation by the same model parameters. Filled symbols are data points; smooth curve is model fit. Open symbols indicate the model prediction for activation at the time of peak current, normalized by the maximal activation at positive potentials, which had an absolute value of 0.18. (*C*) Plot of peak current vs. voltage (filled symbols) for cell N80C. The open symbols indicate the predicted instantaneous current–voltage relation obtained by dividing the measured values of the peak currents by the predicted value of the relative activation (from *B*) at each potential.

We conclude from the results in Fig. 5 that Scheme 3a not only provides a reasonable qualitative model for T-type Ca channel gating, but that it can also explain the kinetic behavior of whole cell T-type currents quantitatively.

Single-Channel Recordings

It would be highly desirable to verify the validity of our model at the single-channel level. Unfortunately, the rapid channel gating and the small unitary conductance of 8 pS in 110 mM Ba have severely hampered our ability to analyze single-channel data quantitatively. However, we can show that within the limits of the resolution of our

TABLE I

Rate Constants Used for Model Calculations with Scheme 3a

$k_a = 6{,}400 \cdot \exp(V/0.00838)$		$k_f = 16{,}000 \cdot \exp(V/0.00838)$
$k_d = 0.502 \cdot \exp(-V/0.00838)$		$k_b = 0.002 \cdot \exp(-V/0.00838)$
$k_o = 3{,}000$	$k_i = 130$	$k_r = 2.5$
$k_c = 750$	$k_{-i} = 0.299$	$k_{-r} = 7.5$

V, membrane potential in volts; rate constants in s^{-1}.

single-channel recordings, the observed unitary activity is consistent with the proposed model. According to the model parameters in Table I, we should observe a single burst of openings for each channel in the membrane. This is expected because the channel should flicker between C_2 and O, but rarely return to C_1, since $k_0 \gg k_d$ even at negative activating voltages. Each burst should be terminated by a transition from O into the inactivated state I_2 and the total open time within a burst should approximate $1/k_i = 7.7$ ms. The mean open time should be independent of voltage and have a value of 1.1 ms. Closings within bursts should be very brief (mean duration = 0.33 ms). Finally, at voltages of submaximal channel activation, the rate of inactivation of the averaged current should be slower than the reciprocal of the mean burst length, and the apparent slowness of inactivation should be caused by late channel openings apparent as a slow latency to first event. If each channel contributes a single burst, the convolution of the first latency with the mean burst length should fit the mean current (Aldrich et al., 1983; Carbone and Lux, 1987*b*; Kirsch and Brown, 1989; Droogmans and Nilius, 1989).

Fig. 6 *A* shows examples of single-channel recordings from a patch which contains three T-type Ca channels, as judged from the maximal number of superimposed openings at positive potentials. As expected from previous studies (Carbone and Lux, 1984; 1987*b*; Nilius et al., 1985; Nowycky et al., 1985; Fox et al., 1987*b*; Chen et al., 1988; Kostyuk et al., 1988; Droogmans and Nilius, 1989), the single-channel current is ~0.3 pA at a test potential of −10 mV with 110 mM Ba as the charge carrier. The average current obtained as the mean of 696 consecutive depolarizations, is similar to the whole-cell T-type Ba current. The time course of the mean single-channel current recorded at −10 mV with 110 mM Ba most closely resembles the whole-cell current obtained at −20 to −30 mV with 20 mM Ba. The difference is most likely a consequence of the shift of channel gating to more positive potentials expected from the effect of the high Ba concentration on external surface charge. The mean open time is 1.6 ms, as shown in Fig. 6 *B*. Since many of the brief closings within a burst are incompletely resolved, concatenation of successive openings must be expected. Therefore we consider the measured value as an upper limit estimate of the true mean open time. We did not find a measurable voltage dependence of the mean open time. However, because of the limited accuracy of our measurements of open times, we cannot conclude from our single-channel data that open times are not voltage dependent.

The occurrence of openings in bursts is clear from the single-channel traces and is further emphasized in the analysis of the closed times. The closed time distribution (Fig. 6 *B*) contains two exponentially decaying components: a very rapid one with an apparent mean duration of 0.56 ms, and a much smaller second component with a mean duration of approximately 20 ms. We interpret the fast component as closings within a burst and the slow one as interburst intervals. According to our model which predicts a single burst per channel, interburst intervals should arise only in sweeps where more than one channel is active. While it is clear that we cannot reliably measure the durations of single openings or closings, we expect less severe errors for the measurement of burst lengths and latencies to first opening. Bursts are well separated (see slow component of closed time histogram) and are little affected by missed short closings. We defined a burst as a series of openings separated by closed

times of less than a critical duration $t = T$. T was obtained from Eq. 2, which describes the time T in a biexponential distribution at which the total number of slow events with duration $t < T$ just equals the total number of short events with duration $t > T$:

$$[1 - \exp(-T/\tau_2)]/\exp(-T/\tau_1) = N_1\tau_1/N_2\tau_2. \quad (2)$$

N and τ are the number of events at time 0 and the time constants for the two exponentials labeled with subscripts 1 (fast) and 2 (slow), respectively. With the

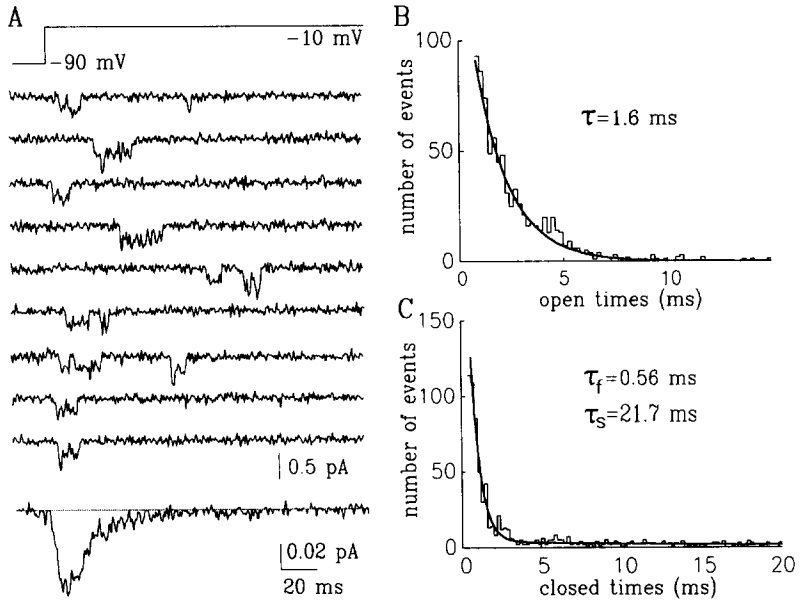

FIGURE 6. Single-channel recordings from T-type Ca channels. (*A*) Cell-attached recording with 110 Ba as the charge carrier. Voltage protocol shown above current traces. Traces with no detectable openings are not shown. The currents were sampled at 5 kHz and filtered at 500 Hz. The trace below the single channel records is the average current obtained from 696 consecutive sweeps. Cell N94A. (*B*) Open time histogram from same patch as in *A*. Smooth curve is single exponential fit with time constant of 1.6 ms. The mean open time must be considered an upper limit estimate because of missed brief closed times. (*C*) Closed time histogram from same patch. Smooth curve is double exponential fit with time constants of 0.56 and 21.7 ms, respectively.

values of N and τ from the closed time histogram shown in Fig. 6 *C*, the value of T was 1.8 ms. The distribution of burst times is shown in Fig. 7 *A*. It can be well fit by a single exponential with a time constant of 6.8 ms.

The cumulative latency to first opening is shown for the same patch in Fig. 7 *B*. We consider measurements of first latency relatively safe, since in our case, where openings occur mainly as bursts, missed events are not a problem. The major source of artifacts is detection of false openings caused by the limited signal-to-noise ratio. Falsely detected openings would tend to shorten the times at which the program

detects the first event. This error cannot account for the result we wish to demonstrate, namely that l. latencies are prolonged and that late occurrence of bursts contributes to the apparent slow rate of inactivation of the averaged current.

The cumulative histogram of first latencies has been normalized to the total

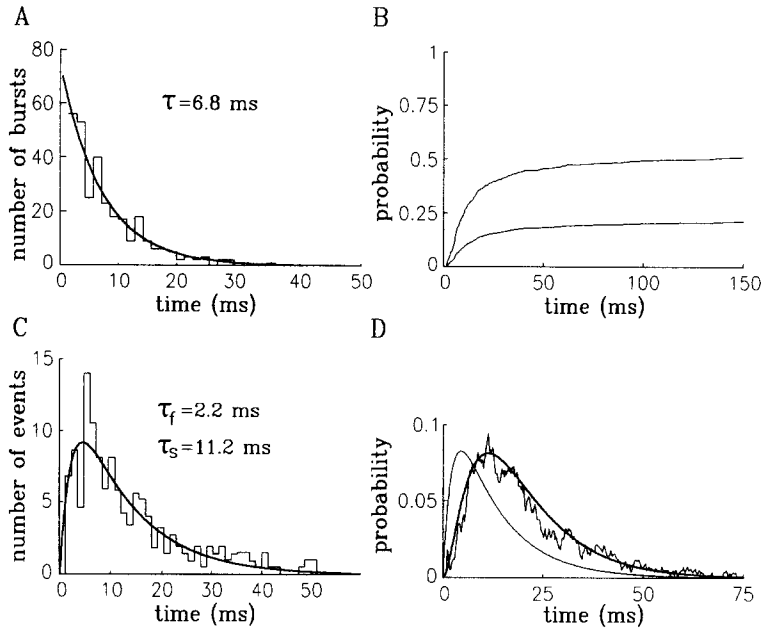

FIGURE 7. Kinetic analysis of single T-type Ca channels. (*A*) Distribution of burst lengths from same patch as in Fig. 6. A burst was defined as a series of openings separated by closed times not exceeding a duration of 1.8 ms (see text for rationale). Smooth line is exponential fit with time constant of 6.8 ms. (*B*) Cumulative histogram of latency to first opening, plotted as probability to open before t by normalization to the total number of sweeps (695) analyzed. Raw data shown as upper curve in *B*. The data indicate that in roughly half the sweeps no openings were detected. The lower curve in *B* is the cumulative histogram to first latency for a single channel obtained by correction of the raw data for the presence of three channels. The correction is $p(1) = 1 - [1 - p(n)]^{1/n}$, where $p(n)$ is the measured probability for n channels and $p(1)$ is the corrected probability for a single channel. (*C*) Histogram of latency to first opening of a single channel obtained from the corrected curve in *B* by numerical differentiation. Smooth curve is fit to $N(t) = N_0 \cdot (\exp[-t/\tau_1) - \exp(-t/\tau_2)]$ with values of $\tau_1 = 2.2$ and $\tau_2 = 11.2$ ms. (*D*) Time course of the open probability obtained from the averaged patch current (noisy trace). For comparison, the time course of the curve fitted to the l. latency in *C* is shown as the smooth curve on the left. The bold smooth curve superimposed on the average current is the result of the convolution of the fitted latency to first opening with the exponential distribution of burst times from *A*.

number of sweeps analyzed. The histogram levels off at a probability to reach the open state of ~0.5, indicating that in this patch, which contained three active channels, openings were detected only in about half the sweeps. Fig. 7 *B* also shows the cumulative first latency corrected for a single channel (Aldrich et al., 1983). The

finding, that for a single channel the probability of reaching the open state levels off at a value of ~0.25, forms the basis for our assignment of the ratio between the rate constants which govern the equilibrium between states C_1 and I_1 in Scheme 3a. With the values of $k_r = 7.5/s$ and $k_{-r} = 2.5/s$, only 25% of channels will be in state C_1 at any point in time, from which they can be activated to reach the open state during a depolarization.

Fig. 7 *C* shows the distribution of l. latencies for a single channel, obtained after differentiation of the corrected cumulative histogram in Fig. 7 *B*. As expected for an activation scheme in which more than one closed state precede the open state, it shows a rising phase and a delayed peak. A fit to a double exponential function yields time constants of 2 and 12 ms, respectively.

We have used the distribution of first latencies in two approaches to test whether the single channel data is compatible with the prediction of our model that each channel gives rise to a single burst before it inactivates.

The first approach consists of a comparison of the time course of the average current with the convolution integral of the distributions of first latencies and burst durations. If each channel only produces a single burst, then this convolution and the averaged current should have similar time courses (Aldrich et al., 1983; Carbone and Lux, 1987*b*; Kirsch and Brown, 1989; Droogmans and Nilius, 1989). As shown in Fig. 7 *D*, this is indeed the case.

In the second approach, we have calculated the expected mean intervals between bursts contributed by several channels, and compared the calculated values with the measured mean duration of long closed times. To calculate these intervals, we have used a random number generator to pick individual first latencies from our measured curve of cumulative first latencies. The difference between any two such values of latencies constitute an expected interval between the time of first opening of two bursts in a trace in which two channels open. A closed time between bursts can then be obtained by subtracting a burst length from the interval between the beginning of the two bursts. Again, a random number generator was used to pick individual burst durations from our measured distribution of burst lengths (Fig. 7 *A*). We calculated a total of 10^6 closed times between bursts. From Fig. 7 *B* we know that the probability for each channel to open in a sweep is 0.25, so from the binomial distribution we expect to observe two and three bursts in 14.06% and 1.56% of current traces, respectively. To account for this, we repeated the above calculation for the case where three channels open in a sweep and added the calculated inter-burst intervals to those obtained with two bursts, in the proportion expected from the binomial distribution. The resulting calculated distribution of intervals between bursts is shown as the thick curve in Fig. 8. Despite the large number of calculated events, the curve is not smooth. This is expected, because l. latencies for the calculation were picked from our measured distribution rather than from a smooth fitted double exponential curve. The calculated curve shows the predicted distribution of closed times which occur as intervals between bursts contributed by three different channels with identical distributions of l. latency. The calculated curve fits the observed distribution of long closed times remarkably well. This provides further strong evidence that each channel only produces a single burst before it inactivates, and supports our model for T-type channel gating.

Comparison between T-Type Channels in Fibroblasts and Neuronal Cells

T-type Ca currents were first described in neurons (Llinas and Yarom, 1981; Carbone and Lux, 1984) and since then have been found in the majority of neuronal cells from which Ca currents have been recorded. Although most of our experimental results on T-type currents in fibroblasts were qualitatively similar to those obtained in neuronal cells, clear quantitative differences also become apparent. This prompted us to compare the two channel types more directly. Fig. 9 *A* shows a series of current records obtained from an NG108 neuroblastoma-glioma cell under similar experimental conditions as those used for the currents in fibroblasts illustrated in Fig. 1. We chose the undifferentiated NG108 cell line because their T-type currents were large compared to the high-threshold activated (L-type and N-type) Ca currents. The most immediately striking difference between T-type currents in fibroblasts and NG108 cells is the much slower time course of inactivation of the neuronal T-type currents. The slower rate of inactivation is observed at every test potential and cannot therefore be explained by a shifted voltage dependence in one

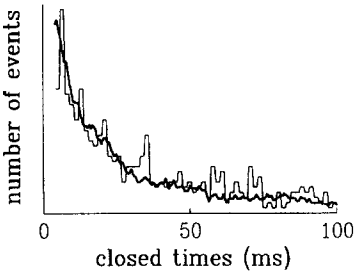

FIGURE 8. Long closed times in multichannel patch are consistent with predicted intervals between single bursts from different channels. Histogram of closed times longer than 3.2 ms from same patch as in Fig. 6. Bold superimposed curve: Predicted distribution of intervals between bursts each resulting from a different channel in a patch containing three channels. The predicted distribution was obtained by calculating a total of 10^6 intervals each resulting from the stochastic occurrence of a single burst from two or three channels opening in the same sweep (see text for details).

of the two channel types. Like its counterpart in fibroblasts, T-type Ca currents in NG108 cells inactive more rapidly at more positive potentials, and the rate of inactivation saturates at potentials positive to −10 mV (Fig. 9 *B*). However, the fastest time constant is about three times slower than that in fibroblasts (compare Figs. 2 and 9). More differences between the channels in fibroblasts and neuronal cells are apparent in Fig. 10. We used the same strategy to obtain quantitative fits to the neuronal T-type currents which had successfully reproduced the kinetic behavior of T-type channels in fibroblasts (see Fig. 5). However, this strategy was not successful for neuronal channels. In Fig. 10 we illustrate the case in which the parameters of our model were adjusted to fit the time course of the current at 0 mV (Fig. 10 *A*). The voltage dependence was then determined from the steady-state inactivation curve (Fig. 10 *B*). Even though steady-state inactivation curves for neuronal T-type currents had a similar midpoint to those in fibroblasts, their steepness was always significantly less. In the example illustrated, the steepness of the inactivation curve could be described by a Boltzmann factor of RT/zF = 6.7 mV, compared with 4.2 mV for the T-type channels in fibroblasts (Fig. 5). This voltage

dependence also gave a reasonable activation curve (see shape of the extrapolated open-channel current–voltage relation in Fig. 10 *C*), but did not provide satisfactory fits to currents at potentials less than 0 mV. Although the rate of activation (and thus the time of the peak currents) could be fitted reasonably well, the predicted rate of inactivation at more negative potentials was much slower than that measured (Fig. 10 *A*). The time course of the current could only have been approximated if the voltage dependence was further decreased, such that at more negative potentials the rate of inactivation was reduced less. In this case, the steady-state inactivation could no longer be fitted, and the activation curve extended to negative potentials at which no currents were observed.

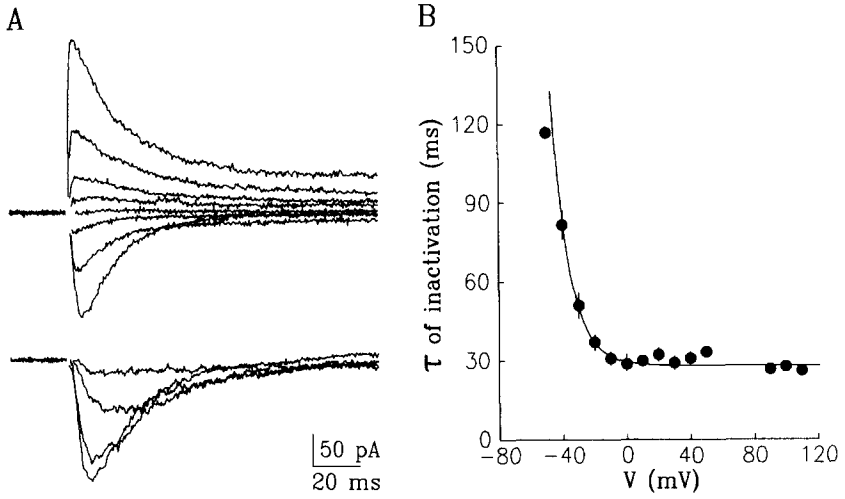

FIGURE 9. T-type currents in undifferentiated NG108 cells. (*A*) Holding potential −90 mV. Lower panel: Superimposed current traces in response to depolarization ranging from −50 mV (smallest current) to −10 mV (largest inward current) in increments of 10 mV. Upper panel: Currents for depolarizations ranging from 0 mV (*bottom trace*) to +140 mV (*top trace*) in increments of 20 mV. Holding potential −90 mV. 20 mM Ba is the charge carrier. The peak of the high threshold activated current remaining at a holding potential of −50 mV in this cell was 10 pA at +20 mV. Cell N01H. (*B*) Plot of the voltage dependence of the time constant of macroscopic inactivation. Data points are means ± SEM from eight cells. The smooth curve indicates an exponential voltage dependence with *e*-fold change per 11 mV and a voltage-independent offset of 30 ms.

We will evaluate possible explanations for the striking differences between neuronal and fibroblast Ca channels in the Discussion. The properties of the T-type currents illustrated in Figs. 9 and 10 are not peculiar to NG108 cells, since we have recorded very similar whole-cell currents from other cells of neuronal origin, including PC12 cells and primary sympathetic neurons. T-type currents were present in the vast majority of NG108 cells (>90%). Consistent with the majority of previous studies (e.g., Wanke et al., 1987; Streit and Lux, 1987; Hirning et al., 1988; Plummer et al., 1989; but see also Garber et al., 1990), only a small percentage of

PC12 cells or rat sympathetic neurons expressed macroscopic T-type currents (<10%). For direct comparison, T-type currents from fibroblasts, NG108 cells and a rat sympathetic neuron are shown in Fig. 11. It is clear that the currents in the two neuronal cells are very similar and differ from their counterparts in fibroblasts. Furthermore, the currents recorded in NG108 cells have the kinetic properties

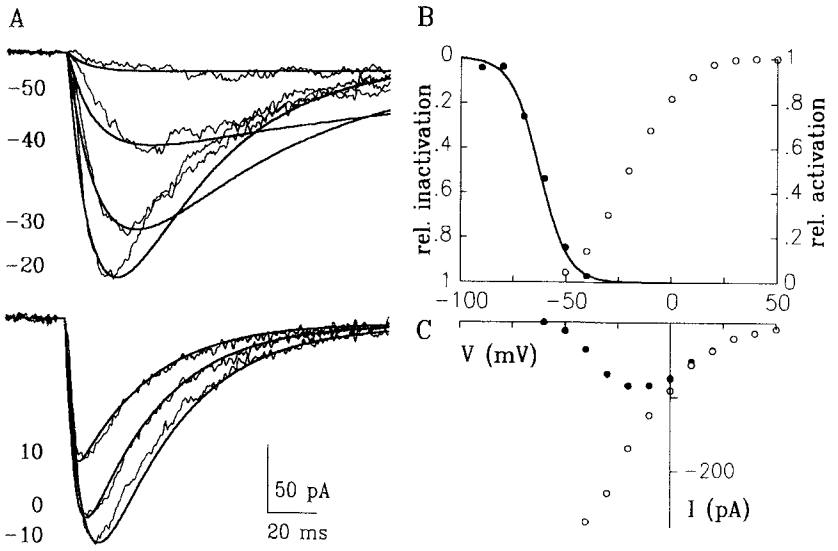

FIGURE 10. The model provides a poor fit to T-type currents in NG108 cells. (*A*) Current records (noisy traces) and superimposed model fits for depolarizations from a holding potential of −90 mV to the test potentials indicated next to each current trace. Data from cell Z07A. Model fit obtained with Scheme 3a (see text) and the following parameters (rate constants in s^{-1}): $k_a = 294 \cdot \exp(V/0.013)$, $k_d = 12.5 \cdot \exp(-V/0.013)$, $k_0 = 1120$, $k_c = 300$, $k_i = 42$, $k_{-i} = 0.17$, $k_r = 1.5$, $k_{-r} = 1.5$, $k_f = 490 \cdot \exp(V/0.013)$, $k_b = 0.023 \cdot \exp(-V/0.013)$ (*B*) Fit of steady-state inactivation by the same model parameters. Filled symbols are data points; smooth curve is model fit. Open symbols indicate the model prediction for activation at the time of peak current, normalized by the maximal activation at positive potentials, which had an absolute value of 0.358. (*C*) Plot of peak current vs. voltage (filled symbols). The open symbols indicate the predicted instantaneous current–voltage relation obtained by dividing the measured values of the peak currents by the predicted value of the relative activation (from *B*) at each potential. Model parameters were chosen to fit the steady-state inactivation curve and the time course of the current at $V = 0$ mV.

previously described for neuronal T-type currents in a variety of tissues (see Table II and Discussion).

DISCUSSION

Gating of T-Type Ca Channels

We have used whole-cell and single-channel recordings to formulate a kinetic model for the gating of T-type Ca channels in 3T3 fibroblasts. 3T3 fibroblasts were well

suited for this purpose because, in many cells, current through T-type Ca channels was the predominant current, particularly after the small L-type currents had run down during prolonged whole cell recording (Carbone and Lux, 1987*a*; Chen et al., 1988; Peres et al., 1988). Even when L-type current was present, the more negative activation range of T-type current allowed recording of the voltage-dependent kinetics of T-type current with little contamination by L-type current.

The kinetic model and its parameters are mostly based on the results of our whole-cell recordings. We used the principle that at extreme potentials voltage-independent rate constants become rate limiting to demonstrate that channel inactivation and channel closing are voltage independent, and that a voltage-independent transition exists in the pathway of recovery of inactivated channels. The rationale for the choice of model parameters can be summarized as follows: (*a*) The microscopic rate of inactivation was assigned the observed saturating rate of macroscopic inactivation at positive potentials. (*b*) The closing rate constant was set by the saturating rate of tail current deactivation at negative potentials. (*c*) The sum

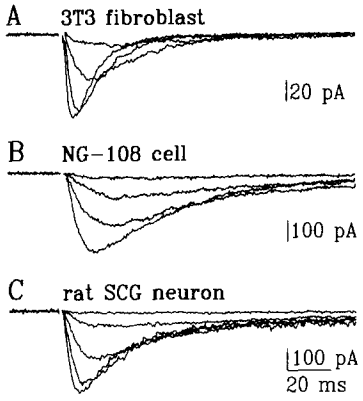

FIGURE 11. Direct comparison of T-type Ba currents in different cell types. (*A*) 3T3 fibroblast (test potentials −50 to −20 mV). Cell N80D: (*B*) NG-108 cell (−50 to −20 mV). Cell Z4A: (*C*) rat SCG neuron (−60 to −20 mV). Cell R41X. Standard solutions (see methods) were used for currents in *A*, *B*, and *C* except $BaCl_2$ was substituted for Ba-acetate in solutions for SCG neurons. Recording *C* was obtained by M. Kanevsky and M. Plummer.

of the voltage-independent rate constants linking states C_1 and I_1 determines the fastest return of inactivated channels to C_1 and was therefore given the value of the saturating rate of recovery at negative potentials. The actual values of the two rate constants were chosen based on the observed fraction of sweeps with detectable openings in single-channel measurements. (*d*) The values of the voltage-dependent rates of activation and deactivation were determined from the fits of the model to the current traces. (*e*) Microscopic reversibility imposed the same voltage dependence along the activating pathway (C_1 to C_2) and along the pathway linking the inactivated states (I_1 to I_2).

The single-channel recordings yielded results consistent with our model, but would not be sufficient by themselves to prove its validity. The results supporting the model are: (*a*) Mean open times (1.6 ms) were similar to the predicted value (1.1 ms), particularly when the effect of missed brief closings is considered. (*b*) Closed times within a burst were too rapid to be resolved faithfully, but the upper limit estimate of 0.56 ms seems compatible with the predicted value of 0.33 ms. (*c*) Mean burst

TABLE II

Comparison of Data in the Literature

		Inactivation									
		Macroscopic decay			Steady state		Deactivation			Recovery from inactivation	
Cell Type	Solutions	τ	V	Asymptote	V1/2	q*	τ	V	Temp (C)	τ	V
	mM	*ms*	*mV*	*ms*	*mV*		*ms*	*mV*	*C*	*ms*	*mV*
3T3 fibroblasts (this paper)	20 Ba	12	−20	8	−65	6	1.4–3	−100 to −70	22	100	−80
3T3 fibroblasts (Peres et al., 1988)	2 Ca	~18	−50	~6	74	5.6			35	220	−80
Myeloma (Fukushima and Hagiwara, 1985)	10 Ca	~50	~−45	~25	~−65						
Smooth muscle (Benham et al., 1987)	110 Ba				−55	5.1					
Cardiac muscle (Hagiwara et al., 1988)	1.8 Ca	25	−60		−75	3.8				144	−80
Cardiac muscle (Bean, 1985)	115 Ba	~30	−20	~12	−41	5.3					
Adrenal gland (Cohen et al., 1988)	20 Ba				−59.8	3.5	8.75	−75	24		
Sensory neurons (Bossu et al., 1985)	5 Ca	30	−20		−48	4.4				285.7–714.3‡	−80
Chick DRG (Carbone and Lux, 1987*a*)	5 Ca	9	10				1.2–5.6	−100 to −70	23	1200	−80
Rat DRG (Fedulova et al., 1985)	2 Ca	75	−55		−80	2.5					
DRG (Fox et al., 1987)	3–10 Ca	20–50		~15–30	−78	5.1					
Hypothalamic (Akaike et al., 1989)	10 Ca	~40	−20	~35	−93					2630	−80
Thalamocortical (Coulter et al., 1989)	3 Ca	~25	−42	~16	−83.5	4				251	−92
Pituitary (Matteson and Armstrong, 1986)	5–30 Ca,Ba	23	20				1.8–3	−100 to −70	17		

*q = equivalent charge, obtained from Boltzman distributions.

‡Time to recover half of maximal current given as 200–500 ms by authors.

lengths (6.8 ms) were similar to the predicted value (7.7 ms). (*d*) Each channel gives rise to a single burst and then inactivates. This was shown by the similarity of the convolution of burst lengths and l. latencies with the mean current, as previously shown by Carbone and Lux (1987*b*) and Droogmans and Nilius (1989). Furthermore, the distribution of long closed times could be predicted correctly with the assumption that long closed times resulted from intervals between bursts from different channels, each of which had the same distribution of latencies to first opening.

The model also predicts that open times and mean bursts lengths should be voltage independent. We were indeed unable to show a change of these parameters with voltage (unpublished data), but the limited voltage range over which a sufficient signal-to-noise ratio could be obtained severely limits the value of these measurements and makes it impossible for us to answer this point conclusively. Carbone and Lux (1987*b*), recording from chick sensory neurons, reported that the mean open time increased slightly with voltage. In contrast, Kostyuk et al. (1988), studying mouse sensory neurons, found an approximately twofold decrease of the mean open time when the test potential was increased from −60 to −30 mV. Droogmans and Nilius (1989) found no voltage dependence of open times in cardiac T-type channels between −40 and 0 mV. None of the above studies attempted to estimate the errors introduced by missed or falsely detected events. Thus, we regard the published evidence for the voltage dependence of mean open times in T-type Ca channels as inconclusive. However, both qualitatively and quantitatively, our results nicely fit with the single channel recordings from cardiac T-type channels recently published by Droogmans and Nilius (1989). We find similar open times, closed times, and burst durations, and our general conclusions about the mechanism of channel gating are also very similar. The only difference remains in the choice of a quantitative model. As we will discuss, our measurements of the rate of recovery from inactivation dictated a cyclic model, and the resulting need to assure microscopic reversibility in any closed loop prevented us from considering models in which the channel can reach the same inactivated state through several parallel transitions (models M5 and M6 in Droogmans and Nilius).

Our model most likely remains an oversimplification of T-type channel gating, particularly inasmuch as the presence of only two closed states is concerned. Nevertheless, with a minimum of ad hoc assumptions, and heavily constrained by a variety of observations, the model provides a surprisingly good fit to our data. For successful modeling of the kinetic pathway from closed to open to inactivated T-type Ca channels it is sufficient to assume voltage dependence only in the early step(s) of activation. Evidence that most of the voltage dependence lies in channel activation and that inactivation is coupled to activation but intrinsically voltage independent has now been presented for several voltage dependent channels, including Na channels (Bezanilla and Armstrong, 1977; Bean, 1981; Aldrich et al., 1983; Gonoi and Hille, 1987; Kirsch and Brown, 1989; Cota and Armstrong, 1989), A-type K channels (Zagotta et al., 1989; Zagotta and Aldrich, 1990) and delayed rectifier K channels (Koren et al., 1990). The apparent similarity of the overall gating mechanism of voltage activated channels is conceptually attractive. It forms a functional correlate to the similar transmembrane topology of voltage-dependent ion channels which has been postulated based on comparisons of the primary sequences and hydropathy profiles of voltage activated Na, K, and Ca channels (for review see Catterall, 1988; Jan and Jan, 1989). The sequence homology is particularly striking within the respective S4 regions, which are generally believed to form the major voltage sensing part of the channel proteins (Noda et al., 1984; Stuehmer et al., 1989; Tosteson et al., 1989).

An additional important conclusion of our kinetic analysis is the finding that the direct opening and closing transitions are not voltage dependent and relatively fast.

A similar claim has recently been made for a delayed rectifier K-channel (Koren et al., 1990) and an A-type K-channel (Zagotta et al., 1989; Zagotta and Aldrich, 1990). Voltage independence of the final opening transition in Na channels has previously been hypothesized (Conti et al., 1984; Conti and Stuehmer, 1989) based on the differential effects of D_2O and hydrostatic pressure on Na channel gating currents and ionic currents (Conti and Palmieri, 1968; Meves, 1974; Schauf and Bullock, 1979; Conti et al, 1984). The emerging picture of the gating mechanism in voltage-dependent channels is thus one in which a number of discrete voltage-dependent transitions occur between closed states. These transitions, which involve a conformational change of a charged part of the channel protein, lead to a permissive, but still closed state, from which the channel can open and/or inactivate through different conformational changes which do not cause net charge movement.

Our model does include a second voltage sensitive transition, namely the equilibrium between the two inactivated states. A priori the simplest model would have been one where only transitions between C_1 and C_2 are voltage dependent, and in which inactivated channels return to C_1 through C_2 in a voltage-independent way. The two possible schemes are the following (Schemes 4 and 5):

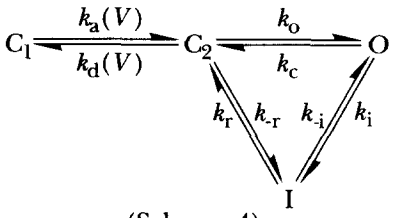

(Scheme 4)

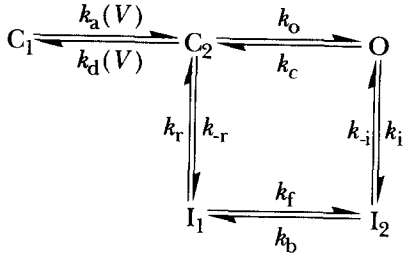

(Scheme 5)

Schemes 4 and 5 could not fit our data for two reasons. First, because the current inactivates almost completely during a pulse, the rate constant for the return to the open state must be ~100 times slower than the forward rate constant leading to I (or I_2). In this case, with the requirement for microscopic balance, Schemes 4 and 5 cannot produce the relatively rapid recovery from inactivation found at negative potentials. Second, with a single pair of voltage-dependent rate constants, the observed voltage range of activation and steady-state inactivation cannot be adequately reproduced.

We have not considered linear schemes in which recovery from inactivation would proceed through the open state. We have no indication for significant channel reopening during recovery from inactivation. Since recovery from inactivation is quite rapid (about two-thirds complete after 100 ms at potentials negative to −80 mV), we should easily have been able to measure a corresponding current during the interpulse interval.

Thus we consider Scheme 3 the simplest one which can adequately describe our data. Our assignment of the second pair of voltage-dependent rate constants to the transitions between the two inactivated states is arbitrary. We could obtain equally

good fits when that equilibrium was assumed to be voltage independent and the voltage dependence was instead assigned to the transition between C_1 and I_1 (Scheme 6).

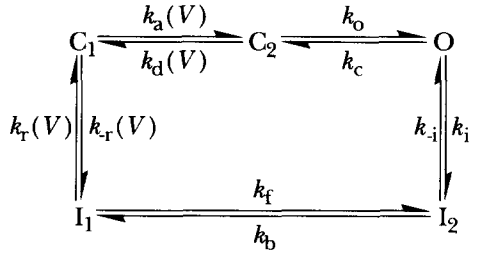

(Scheme 6)

According to Scheme 6, recovery from inactivation at negative potentials should have an initial fast component (rapid recovery of channels which are in state I_1 at the time of repolarization. In contrast, Scheme 3 predicts that recovery from inactivation should be sigmoidal, with an initial delay and a subsequent exponential time course with a time constant equal to the sum of $k_r + k_{-r}$ at negative potentials. We found that within the time resolution of our measurements of the recovery from inactivation (see Fig. 4), we could not differentiate between Schemes 3 and 6. Scheme 3 however appeared more likely, since the first time point of our recovery curves tended to lie below rather than above the monoexponential curves fitted to the rest of the time points.

For reasons of microscopic balance, the overall voltage dependence of the two pairs of voltage-dependent rate constants must be the same. Thus, Scheme 3 is compatible with the interpretation that a change in transmembrane voltage acts on the same voltage sensor whether the channel is in the closed or inactivated state. Our model thus implies that channels exist in a voltage independent equilibrium between available and unavailable conformations. If the channel is in the available conformation (C_1), a change in voltage will open it, whereas the same change in voltage will drag an unavailable channel into I_2 without proceeding through the open conformation.

For simplicity and lack of evidence to the contrary, we assumed that the voltage dependence was equally distributed among the forward and backward rate constants. The best fits were obtained when the forward rate constants were multiplied and the backward rate constants divided by a factor of 3.3 for each 10-mV increase in membrane potential. Thus the equivalent charge q moved across the membrane electric field was

$$q = 2 \cdot \ln(3.3) \cdot (RT/F\Delta V) = 6.0 \text{ electronic charges.}$$

This value is similar to that found by fits of Boltzmann distributions to steady-state inactivation curves of T-type Ca channels in fibroblasts (Peres et al., 1988) and cardiac cells (Bean, 1985), but higher than most estimates for neuronal T-type currents (see Table II and below). The primary structure of T-type Ca channels

remains unknown. Once the sequence becomes available, however, it will be interesting to test which charges can be identified with the voltage sensor. Among the most obvious predictions of our model is the expectation that manipulation of the charges within the voltage sensor should equally affect the steepness of activation and inactivation.

Our data show only minimal overlap of the voltage ranges for steady-state inactivation and activation (Fig. 10). Thus we would expect to observe steady ("window") current only within a very narrow voltage range.

Heterogeneity of T-Type Ca Channels

Although our results on T-type Ca channels in fibroblasts were qualitatively similar to those previously reported for T-type currents in other cells, quantitative differences too large to be accounted for by experimental differences became apparent when we compared our kinetic data to that of previous publications. Figs. 1, 2, 5, and 9–11 and Table II illustrate the differences. The most obvious difference concerns the rate of inactivation, which is more rapid by a factor of 2–3 in fibroblasts (Peres et al., 1988; this paper) than in T-type channels from neuronal cells (see Table II). The difference cannot be explained by shifts along the voltage axis and are thus unlikely to be caused by the different species and concentration of divalent charge carrier. Comparison of Figs. 2 and 9 shows that even under similar experimental conditions, the T-type currents in NG108 cells inactivate more slowly at any potential and reach a voltage independent rate of inactivation at positive voltages which is two to three times slower than the corresponding value in fibroblasts. The recovery from inactivation in neuronal T-type channels is also considerably slower than in fibroblasts (see Table II). The differences were not, however, limited to the kinetic parameters, since steady-state inactivation curves consistently revealed a voltage dependence which was less steep than that found in fibroblast channels. Table II confirms this observation. The equivalent charge obtained from Boltzman fits to steady-state inactivation curves is ~6 for fibroblast channels but ranges between 2.5 and 5 charges for neuronal channels (for references see Table II). We attempted to adapt our model to the neuronal channels by slowing down the individual rate constants as needed. To our surprise, however, we found that we could not find a set of parameters which produced satisfactory fits to neuronal T-type currents. The main problem, as illustrated in Fig. 10, was that once the voltage dependence was fixed, for example by fits of the steady-state inactivation curve, the currents elicited at various test potentials could not be fitted over the entire voltage range.

The most straightforward interpretation of the differences between T-type Ca channels in various tissues is that, like Na, K, and L-type Ca channels, various structurally and functionally distinct isoforms of T-type Ca channels are expressed in different tissues.

The failure to model neuronal T-type currents with our relatively simple scheme could also be accounted for if mechanisms were present in neurons which modified the voltage dependence of channel gating, as proposed by Bean (1989b). In this case an equilibrium between "normal" and modulated channels might be expected, incompatible with the unique set of rate constants in our model. Indeed, a number of reports of modulation of T-type Ca channels in neuronal cells have appeared

recently (Marchetti et al., 1986; Marchetti and Brown, 1988; Bean, 1989*c*), but the mechanism by which channel function is altered remains unknown.

A third explanation for the failure of our model to reproduce neuronal T-type Ca channel currents concerns the possibility that in neuronal cells T-type Ca current cannot be recorded without contamination by other types of Ca currents. Nowycky et al. (1985) and Fox et al. (1987b) have published records of rapidly inactivating Ca currents in DRG neurons which they attribute to N-type channels, but which have a rate of inactivation as fast or faster than that reported for neuronal T-type currents (see Table II). Similar rapidly and completely inactivating currents have recently been recorded from rat nerve terminals isolated from the neurohypophysis by Lemos and Nowycky (1989). According to Fox et al. (1987*a*, *b*) and Lemos and Nowycky (1989), these N-type currents activate at potentials positive to T-type but negative to L-type Ca currents, and show a relatively broad range of steady-state inactivation with a midpoint similar to that of T-type Ca currents. The presence of such currents would make it very difficult to record neuronal T-type Ca currents in isolation over an extended range of potentials. This could account for our inability to fit inactivating neuronal Ca currents with a model which can successfully reproduce the currents in cells in which no evidence for more than a single class of low-threshold-activated, rapidly inactivating Ca channels exists. Neuronal cells therefore may well contain several distinct classes of rapidly inactivating Ca channels which are difficult to dissect at the whole-cell level.

We thank Drs. B. Bean, E. Liman, M. Kanevsky, D. Pietrobon, and M. Plummer for stimulating discussions, and M. Plummer and M. Kanevsky for the recordings from SCG cells.

This work was supported by grants from the U.S. Public Health Service, the American Cancer Society, and the Johnson & Johnson Foundation and a contribution from the Lucille P. Markey Trust.

Original version received 11 October 1989 and accepted version received 15 March 1990.

REFERENCES

Akaike, N., P. G. Kostyuk, and Y. V. Osipchuk. 1989. Dihydropyridine-sensitive low-threshold calcium channels in isolated rat hypothalamic neurones. *Journal of Physiology.* 412:181–195.

Aldrich, R. W., D. P. Corey, and C. F. Stevens. 1983. A reinterpretation of mammalian sodium channel gating based on single channel recording. *Nature.* 306:436–441.

Armstrong, C. M., and D. R. Matteson. 1985. Two distinct populations of calcium channels in a clonal line of pituitary cells. *Science.* 227:65–67.

Beam, K., and C. M. Knudson. 1988. Effect of postnatal development on calcium currents and slow charge movement in mammalian skeletal muscle. *Journal of General Physiology.* 91:799–815.

Bean, B. P. 1981. Sodium channel inactivation in the crayfish giant axon. *Biophysical Journal.* 35:595–614.

Bean, B. P. 1985. Two kinds of calcium channels in canine atrial cells. *Journal of General Physiology.* 86:1–30.

Bean, B. P. 1989*a*. Classes of calcium channels in vertebrate cells. *Annual Reviews of Physiology.* 51:367–384.

Bean, B. P. 1989*b*. Neurotransmitter inhibition of neuronal calcium currents by changes in channel voltage dependence. *Nature.* 340:153–156.

Bean, B. P. 1989*c*. Multiple types of calcium channels in heart muscle and neurons. Modulation by drugs and neurotransmitters. *Annals of the New York Academy of Sciences.* 560:334–345.

Benham, C. D., P. Hess, and R. W. Tsien. 1987. Two types of calcium channels in single smooth muscle cells from rabbit ear artery studied with whole-cell and single-channel recordings. *Circulation Research.* 61 (Suppl. I):10–16.

Bezanilla, F., and C. M. Armstrong. 1977. Inactivation of the sodium channel. I. Sodium current experiments. *Journal of General Physiology.* 70:549–566.

Bossu, J. L., A. Feltz, and J. M. Thomann. 1985. Depolarization elicits two distinct calcium currents in vertebrate sensory neurones. *Pflügers Archiv.* 403:360–368.

Caffrey, J. M., A. M. Brown, and M. D. Schneider. 1987. Mitogens and oncogenes can block the induction of specific voltage-gated ion channels. *Science.* 236:570–573.

Carbone, E., and H. D. Lux. 1984. A low voltage activated, fully inactivating Ca channel in vertebrate sensory neurones. *Nature.* 310:501–511.

Carbone, E., and H. D. Lux. 1987*a*. Kinetics and selectivity of a low-voltage-activated calcium current in chick and rat sensory neurones. *Journal of Physiology.* 386:547–570.

Carbone, E., and H. D. Lux. 1987*b*. Single low-voltage-activated calcium channels in chick and rat sensory neurones. *Journal of Physiology.* 386:571–601.

Catterall, W. A. 1988. Structure and function of voltage-sensitive ion channels. *Science.* 242:50–61.

Chen, C., M. Corbley, T. Roberts, and P. Hess. 1988. Voltage-sensitive calcium channels in normal and transformed 3T3 fibroblasts. *Science.* 239:1024–1026.

Cohen, C. J., R. T. McCarthy, P. Q. Barrett, and H. Rasmussen. 1988. Ca channels in adrenal glomerulosa cells: K^+ and angiotensin II increase T-type Ca channel current. *Proceedings of the National Academy of Sciences.* 85:2412–2416.

Conti, F., I. Inoue, F. Kukita, and W. Stuehmer. 1984. Pressure dependence of sodium gating currents in the squid giant axon. *European Biophysical Journal.* 11:137–147.

Conti, F., and G. Palmieri. 1968. Nerve fiber behavior in heavy water under voltage-clamp. *Biophysik.* 5:71–77.

Conti, F., and W. Stuehmer. 1989. Quantal charge redistributions accompanying the structural transitions of sodium channels. *European Biophysical Journal.* 17:53–59.

Cota, G., and C. M. Armstrong. 1989. Sodium channel gating in clonal pituitary cells: the inactivation step is not voltage dependent. *Journal of General Physiology.* 94:213–232.

Coulter, D. A., J. R. Huguenard, and D. A. Prince. 1989. Calcium currents in rat tholamocortical relay neurones: kinetic properties of the transient, low-threshold current. *Journal of Physiology.* 414:587–604.

DeRiemer, S. A., and B. Sakmann. 1986. Two calcium currents in normal rat anterior pituitary cells identified by a plaque assay. *Experimental Brain Research Series.* 14:139–154.

Droogmans, G., and B. Nilius. 1989. Kinetic properties of the cardiac T-type calcium channel in the guinea-pig. *Journal of Physiology.* 419:627–650.

Fedulova, S. A., P. G. Kostyuk, and N. S. Veselovsky. 1985. Two types of calcium channels in the somatic membrane of new-born rat dorsal root ganglion neurones. *Journal of Physiology.* 359:431–446.

Fox, A. P., M. C. Nowycky, and R. W. Tsien. 1987*a*. Kinetic and pharmacological properties distinguishing three types of calcium currents in chick sensory neurones. *Journal of Physiology.* 394:149–172.

Fox, A. P., M. C. Nowycky, and R. W. Tsien. 1987*b*. Single channel recordings of three types of calcium channels in chick sensory neurones. *Journal of Physiology.* 394:173–200.

Fukushima, Y., and S. Hagiwara. 1985. Currents carried by monovalent cations through calcium channels in mouse neoplastic B lymphocytes. *Journal of Physiology.* 358:255–284.

Garber, S. S., T. Hoshi, and R. Aldrich. 1989. Regulation of ionic currents in pheochromocytoma cells by nerve growth factor and dexamethasone. *Journal of Neuroscience.* 9:3976–3987.

Gonoi, T., and B. Hille. 1987. Gating of Na channels. Inactivation modifiers discriminate among models. *Journal of General Physiology.* 89:253–274.

Hagiwara, N., H. Irisawa, and M. Kameyama. 1988. Contribution of two types of calcium currents to the pacemaker potentials of rabbit sino-atrial node cells. *Journal of Physiology.* 395:233–253.

Hamill, O. P., A. Marty, E. Neher, B. Sakmann, and F. J. Sigworth. 1981. Improved patch-clamp techniques for high-resolution current recording from cells and cell-free membrane patches. *Pflügers Archiv.* 391:85–100.

Hess, P. 1990. Calcium channels in vertebrate cells. *Annual Reviews in Neuroscience.* 13:337–356.

Hess, P., J. B. Lansman, and R. W. Tsien. 1986. Calcium channel selectivity for divalent and monovalent cations. *Journal of General Physiology.* 88:293–319.

Hirning, L. D., A. P. Fox, E. W. McCleskey, B. M. Olivera, S. A. Thayer, R. J. Miller, and R. W. Tsien. 1988. Dominant role of N-type Ca^{2+} channels in evoked release of norepinephrine from sympathetic neurons. *Science.* 239:57–61.

Hodgkin, A. L., and A. F. Huxley. 1952. A quantitative description of membrane current and its application to conduction and excitation in nerve. *Journal of Physiology.* 117:500–544.

Jan, L. Y., and Y. N. Jan. 1989. Voltage-sensitive ion channels. *Cell.* 56:13–25.

King, E. L., and C. Altman. 1956. A schematic method of deriving the rate laws for enzyme-catalyzed reactions. *Journal of Physical Chemistry.* 60:1375–1378.

Kirsch, G. E., and A. M. Brown. 1989. Kinetic properties of single sodium channels in rat heart and rat brain. *Journal of General Physiology.* 93:85–99.

Koren, G., E. R. Liman, D. E. Logothetis, B. Nadal-Ginard, and P. Hess. 1990. Gating mechanism of a cloned K-channel expressed in frog oocytes and mammalian cells. *Neuron.* 4:39–51.

Kostyuk, P. G., Y. M. Shuba, and A. N. Savchenko. 1988. Three types of calcium channels in the membrane of mouse sensory neurons. *Pfluegers Archiv.* 411:611–669.

Lemos, J. R., and M. C. Nowycky. 1989. Two types of calcium channels coexist in peptide-releasing vertebrate nerve terminals. *Neuron.* 5:1419–1426.

Llinas, R., and Y. Yarom. 1981. Properties and distribution of ionic conductances generating electroresponsiveness of mammalian inferior olivary neurons in vitro. *Journal of Physiology.* 315:569–584.

Marchetti, C., and A. M. Brown. 1988. Protein kinase activator 1-oleoyl-2-acetyl-sn-glycerol inhibits two types of calcium currents in GH3 cells. *American Journal of Physiology.* 254:C206–C210.

Marchetti, C., E. Carbone, and H. D. Lux. 1986. Effects of dopamine and noradrenaline on Ca channels of cultured sensory and sympathetic neurons of chick. *Pfluegers Archiv.* 406:104–111.

Matteson, D. R., and C. M. Armstrong. 1986. Properties of two types of calcium channels in clonal pituitary cells. *Journal of General Physiology.* 87:161–182.

Meves, H. 1974. The effect of holding potential on the asymmetry currents in squid giant axons. *Journal of Physiology.* 243:847–867.

Nilius, B., P. Hess, J. B. Lansman, and R. W. Tsien. 1985. A novel type of cardiac calcium channel in ventricular cells. *Nature.* 316:443–446.

Noda, M., S. Shimizu, T. Tanabe, T. Takai, T. Kayano, T. Ikeda, H. Takahashi, H. Nakayama, Y. Kanaoka, N. Minamino, K. Kangawa, H. Matsu, M. A. Raftery, T. Hirose, S. Inayama, H. Hayashida, T. Miyata, and S. Numa. 1984. Primary structure of Electrophorus electricus sodium channel deduced from cDNA sequence. *Nature.* 312:121–127.

Nowycky, M. C., A. P. Fox, and R. W. Tsien. 1985. Three types of neuronal calcium channel with different calcium agonist sensitivity. *Nature.* 316:440–443.

Peres, A., R. Zippel, E. Sturani, and G. Mastacciuolo. 1988. Properties of the voltage-dependent calcium channel of mouse Swiss 3T3 fibroblasts. *Journal of Physiology.* 401:639–655.

Plummer, M. R., D. E. Logothetis, and P. Hess. 1989. Elementary properties and pharmacological sensitivities of calcium channels in mammalian peripheral neurons. *Neuron.* 2:1453–1463.

Schauf, C. L., and J. O. Bullock. 1979. Modification of sodium channel gating in Nyxicola giant axons by deuterium oxide, temperature, and internal cations. *Biophysical Journal.* 27:193–208.

Streit, J., and H. D. Lux. 1987. Voltage-dependent calcium currents in PC12 growth cones and cells during NGF-induced cell growth. *Pflügers Archiv.* 408:634–641.

Stuehmer, W., F. Conti, H. Suzuki, S.Wang, M. Noda, N. Yahagi, H. Kubo, and S. Numa. 1989. Structural parts involved in activation and inactivation of the sodium channel. *Nature.* 339:597–603.

Sturek, M., and K. Hermsmeyer. 1986. Calcium and sodium channels in spontaneously contracting vascular muscle cells. *Science.* 233:475–478.

Tosteson, M. T., D. S. Auld, and D. C. Tosteson. 1989. Voltage gated channels formed in lipid bilayers by a positively charged segment of the Na channel polypeptide. *Proceedings of the National Academy of Sciences.* 86:707–710.

Tsien, R. W., D. Lipscombe, D. V. Madison, K. R. Bley, and A. P. Fox. 1988. Multiple types of neuronal calcium channels and their selective modulation. *Trends in Neuroscience.* 11:431–438.

Wanke, E., A. Ferroni, A. Malgaroli, A. Ambrosini, T. Pozzan, and J. Meldolesi. 1987. Activation of a muscarinic receptor selectively inhibits a rapidly inactivated Ca^{2+} current in rat sympathetic neurons. *Proceedings of the National Academy of Sciences.* 84:4313–4317.

Yaari, Y., B. Hamon, and H. D. Lux. 1987. Development of two types of calcium channels in cultured mammalian hippocampal neurons. *Science.* 235:680–682.

Zagotta, W. N., and R. W. Aldrich. 1990. Voltage-dependent gating of Shaker A-type potassium channels in *Drosophila* muscle. *Journal of General Physiology.* 95:29–69.

Zagotta, W. N., T. Hoshi, and R. W. Aldrich. 1989. Gating of single Shaker potassium channels in *Drosophila* muscle and in *Xenopus* oocytes injected with Shaker mRNA. *Proceedings of the National Academy of Sciences.* 86:7243–7247.